INTERNATIONAL JOURNAL OF
COASTAL & OFFSHORE ENGINEERING
IJCOE Vol.2/No. 2/Spring 2017 (41-50)

Available online at: http://ijcoe.org/browse.php?a_code=A-10-53-1&sid=1&slc_lang=en

Simulating Regular Wave Interaction with Structures in Two-Dimensions Using a Modified WCSPH

Ehsan Delavari [1], Ahmad Reza Mostafa Gharabaghi [2*]

[1] *Ph.D. Candidate, Faculty of Civil Engineering, Sahand University of Technology, Tabriz, Iran*
[2*] *Professor, Faculty of Civil Engineering, Sahand University of Technology, Tabriz, Iran*

ARTICLE INFO

Article History:
Received: 9 Jan. 2017
Accepted: 22 Jul. 2017

Keywords:
Wave-structure interaction
Rigid body
Regular wave
Weakly compressible SPH

ABSTRACT

A weakly compressible SPH (WCSPH) scheme has been developed to simulate interaction between waves and rigid bodies. The developed WCSPH scheme is improved by applying a modified equation to calculate the wave-structure interaction, in order to increase its accuracy. The effects of relative fluid/solid particles' acceleration are considered in the modified equation. To evaluate the efficiency of developed model, the dynamics of structural movements and related pressure fields are investigated for several test cases and the results are compared with the experimental data. It seems that the modified algorithm is able to improve the accuracy of simulated wave-structure interactions.

1. Introduction

Simulation of the wave-structure interaction is one of the interesting fields in ocean engineering. Due to the difficulties and complications of the problem, majority of the studies in this field are based on the experimental and/or numerical methods.

Greenhow and Lin (1983) performed some experiments on the high speed entry of a wedge and cylinder into calm water. The dead-rise angels of the tested wedges were 81, 75, 60, 45, and 30 degrees. The depth of penetration, velocity of the wedge, and deformed shape of the free surface are some of the data recorded by them. Loverty (2004) performed an experimental study to investigate the hydrodynamics of spherical projectiles impacting the tranquil free surface of water. In another work, the pressure distribution on free falling wedge entering calm water was studied by Yettou et al. (2006). They performed some experiments on different wedges with five dead-rise angels, two drop heights, and four additional masses. Among the experimental studies, some studies have been performed on the water wave effects on the floating structures. Tolba (1998) experimentally investigated the performance of a rectangular floating breakwater under regular wave actions in intermediate and deep water. His experiments were consisted of restrained (fixed) and pile supported models as well as models with limited roll motion. In another work, Jung (2004) investigated the interactions between regular waves and a rectangular barge, experimentally. The barge was fixed in such a way that it could just roll (one degree of freedom).

Moreover in literature, there are a number of studies evaluating the mutual behavior of fluid and structure numerically. Most of the applied numerical methods for investigation of the wave-structure and/or generally fluid-structure interactions are generally based on potential flow theory like boundary element method (BEM) (for example, Sun and Fultinsen,2006) and Mixed Eulerian-Lagrangian Boundary element method (MEL-BEM) (for example, Fultinsen, 1977, and Koo, 2003). This is due to the complexity of problems dealing with the wave-structure interaction. Applying potential theory based methods for such problems need some simplifying assumptions (like incompressible/non-viscous fluid, irrotational flow, etc.) that may affect the accuracy of the results. Currently, some simple solver methods for Navier-Stokes' equations such as Smoothed Particle Hydrodynamic (SPH) scheme have been developed. Kajtar and Monaghan (2008) simulated the swimming of three linked-rigid bodies using WCSPH method. They integrated the interaction equations by a second-order method which conserves linear momentum exactly. In another work, Monaghan and Kajtar (2009) developed a new force equation for modeling the boundaries. In the proposed method, they modeled the boundaries by means of boundary particles which exert forces on a fluid. They showed that, when the boundary particle's spacing is at least 2 times less than the fluid particle's spacing, the proposed

equation gives good results. Based on this work, Kajtar and Monaghan (2010) studied the motion of three linked ellipses moving through a viscous fluid in two dimensions. Hashemi et al. (2012) developed a WCSPH scheme with a new no-slip boundary condition to simulate rigid body movements in fluids. Omidvar et al. (2012, 2013) used a WCSPH method with a variable particle mass distribution technique to simulate interactions between waves and fixed and moving structures. They used a finer resolution near the structure and a coarser one in the other parts of the domain. Gao et al. (2012) investigated the regular wave slamming on an open-piled structure by WCSPH method. They used an improved wall particle treatment to track impacting characteristics around the structure. An explicit synchronous algorithm for computing the fully coupled viscous fluid-solid interactions was introduced by Bouscasse et al. (2013). They also developed a dedicated algorithm to manage the intersection between the free surface and the solid body. They used a ghost-fluid technique with no-slip boundary condition. Cao et al. (2014) investigated the characteristics of the sloshing liquid loads in a tank. They used a novel boundary treatment considering the boundary motion. Liu et al. (2014) studied the interaction between free surface flows with moving rigid bodies. They improved the WCSPH model with corrections on the SPH kernel and kernel gradients, improvement of solid boundary condition, and application of Reynolds-averaged Navier-Stokes turbulence model. A modified dynamic solid boundary treatment (MDSBT) was proposed by Ni et al. (2014) in order to solve the fluid boundary separation problem. In another work, Sun et al. (2015) applied an improved version of WCSPH method to simulate violent interaction between free surface and rigid body. They improved dummy particle technique for stationary and moving boundary so the calculation of forces and torques on rigid body is improved for higher accuracy. Ren et al. (2015) investigated the nonlinear interactions between waves and floating bodies using an improved WCSPH scheme. Their improved algorithm was based on the dynamic boundary particles (DBPs) to treat the moving boundary of the floating body. Yan et al. (2015) studied the motion of a wedge and catamaran shaped hulls in two dimensions. They used a SPH scheme suitable for two-phase flow for simulating the body impact to the water surface. In another work, the efficiencies of two popular solid wall boundaries were studied by Valizadeh and Monaghan (2015). They compared the results of boundary force method Monaghan and Kajtar and fixed boundary particles of Morris et al. (1997) and Adami et al. (2012).

In spite of several attempts to resolve the deficiencies of SPH based models for fluid/solid interaction, there are still shortages in modeling violent movements of the fluid/solid particles. In this paper, the repulsive force boundary method proposed by Monaghan and Kajtar (2009) has been modified in order to consider the effects of both fluid/solid particles' acceleration. The modified model is verified by simulating the violent interactions between waves and structures, therefore four test cases are simulated using WCSPH scheme and the results are compared with the experimental data.

2. Weakly compressible SPH scheme

For simulation of a weakly-compressible, viscous fluid, the well-known Navier-Stokes' equations are solved. These equations can be written in a Lagrangian form as:

$$\frac{\mathrm{d}\rho}{\mathrm{d}t} = -\rho\nabla.\mathbf{u} \tag{1}$$

$$\frac{\mathrm{d}\mathbf{u}}{\mathrm{d}t} = -\frac{1}{\rho}\nabla p + \nu\nabla^2\mathbf{u} + \mathbf{b} \tag{2}$$

where $\mathbf{u}$ is the fluid velocity vector, ρ is the fluid density, p is the pressure, $\mathbf{b}$ is the body force vector (e.g. gravity force) and ν is the kinematic viscosity considered as equal to $1\times10^{-6}m^2/s$. In the SPH scheme, the fluid domain is discretized as a finite number of particles. Each of these particles represents a small volume of the fluid domain having its own physical properties. For particle i, the discretized SPH form of the governing equations can be written, by exerting a summation on the neighboring particles j, as:

$$\frac{D\rho_i}{Dt} = \sum_{j=1}^{N} m_j\left(\mathbf{u}_i - \mathbf{u}_j\right).\nabla_i W_{ij} \tag{3}$$

$$\frac{D\mathbf{u}_i}{Dt} = -\sum_{j=1}^{N} m_j\left(\frac{p_i}{\rho_i^2} + \frac{p_j}{\rho_j^2} + R\left(f_{ij}\right)^4\right)\nabla_i W_{ij} + \nu(\nabla^2\mathbf{u})_i + \mathbf{b}_i \tag{4}$$

Also:

$$\frac{D\mathbf{r}_i}{Dt} = \mathbf{u}_i \tag{5}$$

In equations (3)-(5), m is the mass, $\mathbf{r}$ is the position vector, and W is a smoothing kernel function. In this paper, the cubic spline kernel was used as the kernel function. According to a study performed by Cao et al. (2014), the cubic spline function has a reasonable accuracy. In addition, due to its smaller coefficient for the smoothing length, it needs a smaller computational time. The cubic spline function is given by (Monaghan and Lattanzio 1985):

$$W(q,h) = \alpha_d\begin{cases}1-\frac{3}{2}q^2+\frac{3}{4}q^3, & 0\le q<1\\ \frac{1}{4}(2-q)^3, & 1\le q<2\\ 0, & q\ge 2\end{cases} \tag{6}$$

where $q = r/h$, h is the smoothing length, r is the distance between the particles i and j and $\alpha_d =$

$10/7\pi h^2$ for 2-D cases (Fig. 1). Term $R(f_{ij})^4$ in Eq. (4) is the artificial pressure term introduced by Monaghan (2000) to remove the tensile instability problem.

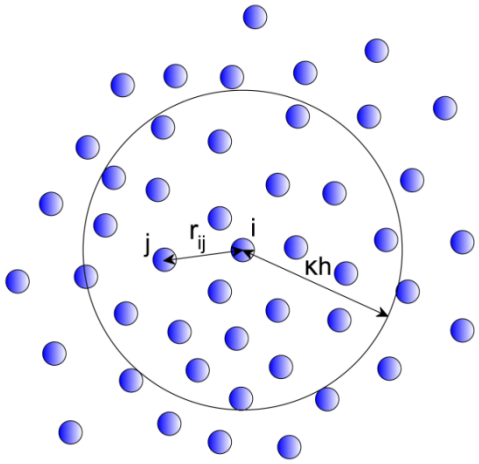

Figure 1. Schematic sketch of SPH particle approximation and the smoothing length

A density re-initialization technique was used by applying a zero order Shepard filter on the density field every 20 time steps in order to reduce the artificial density fluctuations. It was investigated that for time steps larger than 20, the effect of re-initialization can be ignored. In other words, every 20 time step, the new density is estimated as follows (Gomez-Gesteria et al. 2012):

$$\rho_i^{new} = \sum_{j=1}^{N} m_j \widetilde{W}_{ij} \tag{7}$$

in which:

$$\widetilde{W}_{ij} = W_{ij} / \sum_j W_{ij} \frac{m_j}{\rho_j} \tag{8}$$

In the developed WCSPH scheme, the pressure field is calculated by an equation of state relating the density field directly to the pressure field. In this study, the equation of state introduced by Monaghan (1994) is used that imposes very low density variations and is efficient for calculation, which is given by:

$$p = \frac{{c_0}^2 \rho_0}{\gamma}\left[\left(\frac{\rho}{\rho_0}\right)^{\gamma} - 1\right] \tag{9}$$

where c_0 is the sound speed, ρ_0 is the reference density (here, $\rho_0 = 1000\, kg/m^3$), and $\gamma = 7$. In order to enforce the weak-compressibility, a numerical speed of sound c_0 is introduced which is usually adopted as ten times larger than the maximum fluid velocity in the flow field (Monaghan, 1994) due to computational reasons. The magnitude of this parameter is very lower than its real value and is chosen in such a way that ensures the fluid density variations to be less than one percent in the flow field. To calculate the viscous force term in Eq. (4), the equation introduced by Lo and Shao (2002) was used:

$$\nu(\nabla^2 \mathbf{u})_i = \sum_j m_j \frac{4(\mu_i+\mu_j)}{(\rho_i+\rho_j)^2} \frac{\mathbf{r}_{ij}.\nabla_i W_{ij}}{(r_{ij}^2+\eta^2)} \mathbf{u}_{ij} \tag{10}$$

where μ is the dynamic viscosity of the fluid, $\mathbf{r}$ is the position vector, $\mathbf{r}_{ij} = \mathbf{r}_i - \mathbf{r}_j$, $\mathbf{u}_{ij} = \mathbf{u}_i - \mathbf{u}_j$, r_{ij} is the magnitude of the position vector between particles i and j, and $\eta = 0.1h$.

3. Fluid-solid interaction

The solid dynamics is simulated by the second law of Newton. Linear and angular momentum equations are given in two-dimensional framework as:

$$M \frac{d\mathbf{V}_g}{dt} = M\mathbf{g} + \mathbf{F}_{fluid-body} \tag{11}$$

$$I_g \frac{d\Omega_g}{dt} = \mathbf{k}.\mathbf{T}_{fluid-body} \tag{12}$$

where index g refers to parameters which belong to the center of gravity of the solid body, $\mathbf{V}_g$ and Ω_g are the velocity vector and the angular velocity of the center of gravity of the studied body, M and I_g are the mass and the moment of inertia of the body with respect to its center of gravity. $\mathbf{g}$ is the gravity acceleration vector. $\mathbf{F}_{fluid-body}$ and $\mathbf{T}_{fluid-body}$ are the vector of fluid-body hydrodynamic force and torque, respectively, and $\mathbf{k}$ is the unit vector normal to the *xy*-plane.

Among the equations used for calculating the hydrodynamic forces in the SPH scheme, the equation proposed by Monaghan and Kajtar (2009) is a simple and efficient one. It can be written in the form of the following equations:

$$\mathbf{F}_i = \sum_b m_b [\sum_i (\mathbf{f}_{bi} - \nu(\nabla^2 \mathbf{u})_b)] \tag{13}$$

in which:

$$\mathbf{f}_{bi} = \frac{\alpha}{\beta} \frac{\mathbf{r}_{bi}}{(r_{bi} - \frac{dp}{\beta})^2} K(r_{bi}/h) \frac{2m_i}{m_b+m_i} \tag{14}$$

In these relations, subscript i and b are related to the fluid and solid particles, respectively (Fig. 2), dp is the initial fluid particle spacing, β is ratio of the fluid particles' spacing to the solid particles' spacing, and α is a constant and its value depends on the maximum velocity of fluid in the computational domain, $\nu(\nabla^2 \mathbf{u})_b$ is the viscous force given by equation (10), $\mathbf{f}_{bi}$ is the force on solid particle b due to the fluid particle i and $K(r_{bi}/h)$ is a 1D kernel function. In this point, the Wendland 1D quantic function is used which is given as (Monaghan and Kajtar 2009):

$$K(q) = \begin{cases} w_5 \left(1 + \frac{5}{2}q + 2q^2\right)(2-q)^5 & 0 \le q \le 2 \\ 0 & q > 2 \end{cases} \tag{15}$$

in which w_5 is a constant which its value is chosen such that $K(0) = 1$ (Kajtar, 2009).

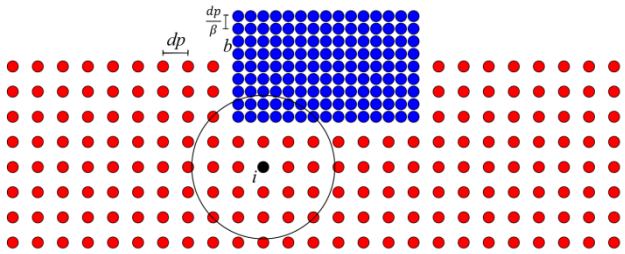

Figure 2. Interaction between fluids (red) and solid (blue) particles

The equation proposed by Monaghan and Kajtar (2009) is almost accurate in simulating interaction forces between fluid and structure. But its accuracy decreases in the violent situations such as wave-body interaction problem, because the effects of the structure acceleration have not been considered in the original equation. Consequently, a modified form of the equation is introduced in order to consider the motion of fluid and rigid body, simultaneously. The modified equation is given as:

$$\mathbf{f}_{bi} = \frac{\alpha}{\beta}\frac{\boldsymbol{r}_{bi}}{(r_{bi}-\frac{dp}{\beta})^2}K(r_{bi}/h)\frac{2m_i}{m_b+m_i} + (\mathbf{b}-\mathbf{a}_i)W_{bi}\frac{m_i}{\rho_i} \quad (17)$$

b is the body force per mass vector that in the test cases investigated here, it is the gravitational acceleration. The value of α related to the first term is considered different in x and y directions. This is due to the differences in the velocities of the fluid in x and y directions in wave domain. Therefore, it can be written as:

$$\alpha_x = \varphi\alpha_y \quad (18)$$

in which φ is a constant and $\varphi \geq 1$. The value of parameter φ is different for any test case and it can be determined with a trial and error process. In this study, in all of test cases it is considered to be equal to 1.10.

4. Numerical tests

Four test cases are developed here to evaluate the performance of the modified force interaction equation in simulating violent wave-structure interaction problems. First, a lid-driven cavity problem is simulated, as a benchmark case, to evaluate the viscous model. As a second case, in order to evaluate the modified equation in simulating wedge impact problems, a test case on the water entry of a wedge is studied. The hydrodynamic characteristics of a rectangular barge with just roll degree of freedom are investigated as the third case. In the last case, the movements and pressure distribution on a pile-supported floating breakwater are simulated by the developed WCSPH algorithm.

4.1. Lid-driven cavity

The lid-driven cavity is a benchmark test case for evaluating the accuracy of the no-slip solid wall boundary. The numerical results of Ghia et al. (1982) are used as the reference data. The length and width of the square cavity (L) is normalized to 1. The top wall of the cavity moves with a constant normalized velocity of 1 and all the other boundaries are at rest (Fig. 3). The kinematic viscosity of the fluid (υ) is assumed to be 0.001 and as a result, the Reynolds number is equal to 1000. The initial density of the fluid is set to 1. The applied smoothing length is equal to $1.33dx$ (dx is the initial particle spacing), and a fourth order Runge-Kutta scheme is used as a numerical integrator. Evaluating the convergence of the numerical model, three particle resolutions of 50×50, 100×100, and 200×200 are used. At $t = 60\,s$, the fluid flow becomes steady and the horizontal and vertical velocities at the middle section of the cavity ($x = 0.5$ and $y = 0.5$) are evaluated. Fig. 4 shows the variations of the estimated velocities with the results reported by Ghia et al. (1982). It can be seen that the SPH results obtained from resolutions of 100×100 and 200×200 are in good agreement.

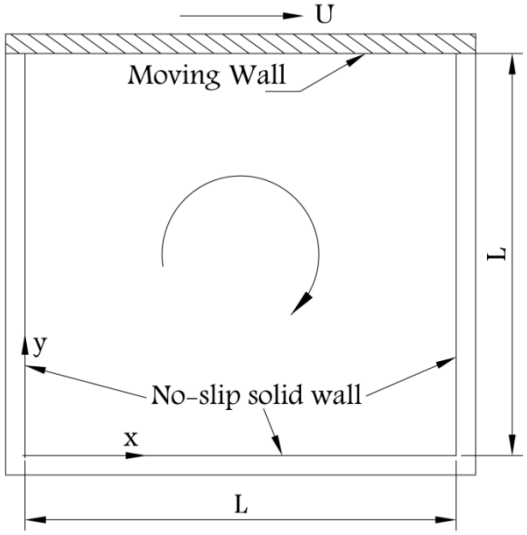

Figure 3. Schematic sketch of the lid-driven cavity problem

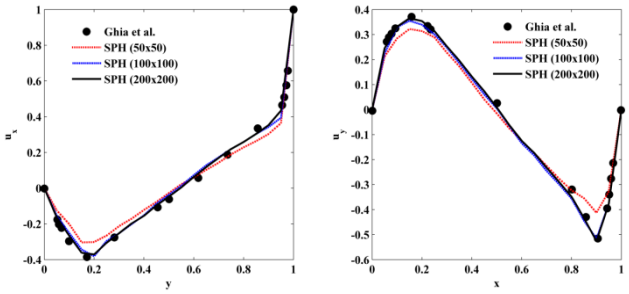

Fig. 4. Velocity profiles on $x = 0.5$ (left panel) and $y = 0.5$ (right panel)

4.2. Wedge Water Entry

A sailing boat or containership in rough waters will experience extremely high slamming forces due to the coupling effects of the ship and the induced waves. The applied pressure on the bottom of the ship can damage the ship structure. This is one of the violent fluid-solid interaction problems and its simulation is very complex. Usually the ship bottom is simplified

by a 2-D symmetrical wedge shape which entries to the free surface with an initial velocity. Therefore, in the next step, an experimental case performed by Yang et al. (2007) is studied. A 2D wedge section with a deadrise angle of $\theta = 10°$ at the bottom, and 0.6 m in width is dropped just from touching the free surface with an initial velocity of 1.83 m/s. The mass of the wedge is 60 kg. The basin is 1.5 m in width with a water depth of 0.6 m. To eliminate the effects of walls, a sponge layer (Delavari and Gharabaghi, 2014) is applied at all sides of the numerical basin (Fig. 5). In the SPH model, the initial particle spacing is 0.002 m with a smoothing length equal to $1.33dx$, and a fourth order Runge-Kutta scheme is used as a numerical integrator. The numerical results are compared with the experimental data from Yang et al. (2007).

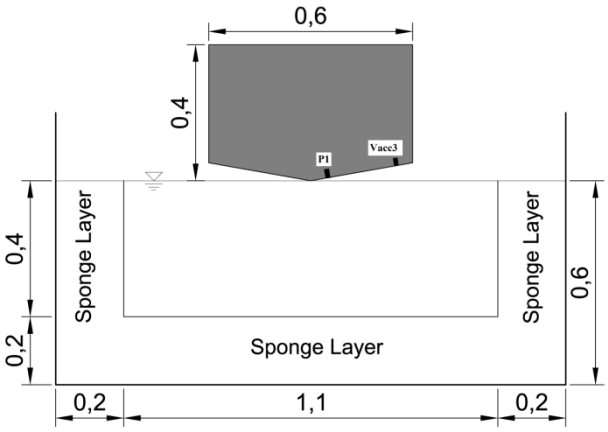

Figure 5. Schematic sketch of the numerical model

A comparison between the accelerations and velocities of the wedge obtained from the numerical model and experimental data obtained from accelerometer Vacc3, located 250 mm off from the model centerline, has been shown in Fig. 6 and 7. According to the experimental data, it is assumed that the impact moment occurs at $t = 2.868\ s$. As can be seen, the results of both modified and unmodified models are in good agreement with the experimental data. At the initial stages of the simulation, the modified model is more accurate. But with decreasing the violent condition, the results of both models are almost identical.

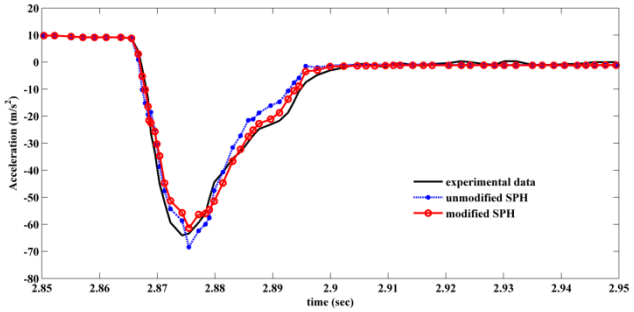

Figure 6. Time history of vertical acceleration of the wedge obtained from the numerical models compared with the experimental data from Yang et al. (2007)

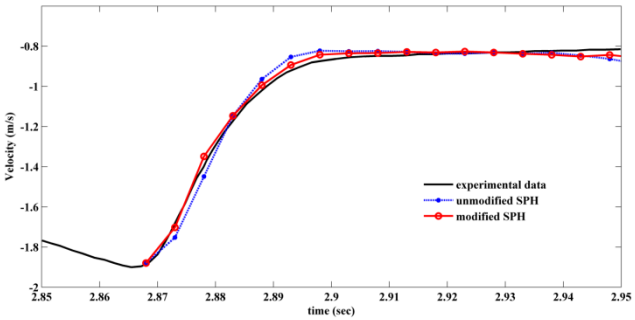

Figure 7. Time history of vertical velocity of the wedge obtained from the numerical models compared with the experimental data from Yang et al. (2007)

A snapshot of the numerical pressures and velocities of the fluid particles simulated by the modified SPH, at $t = 2.928\ s$ has been shown in Figs. 8 and 9.

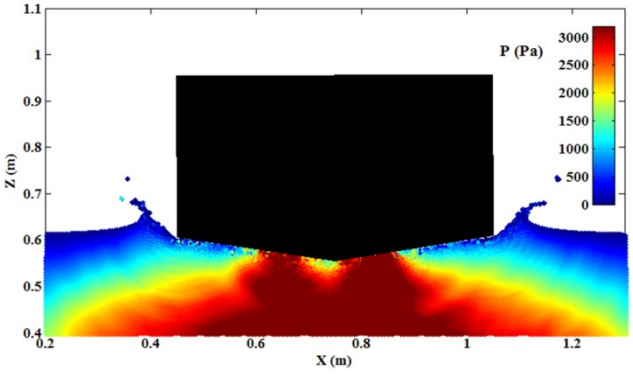

Figure 8. A snapshot of the numerical pressures simulated by the modified SPH scheme at $t = 2.928\ s$

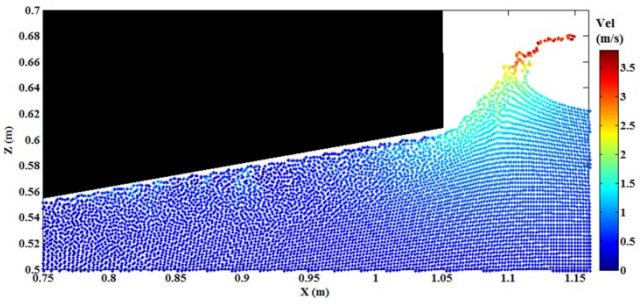

Fig. 9. A snapshot of the numerical velocities of the fluid particles simulated by the modified SPH scheme at $t = 2.928\ s$

In Fig. 10, time history of the estimated pressure at pressure gage P1 from the numerical models, located 50 mm off from the model centerline, have been compared with the experimental data from Yang et al. (2007). The numerical pressures at gage P1 have been calculated by an average SPH summation $P_s = \sum_f P_f W_{sf} / \sum_f W_{sf}$ where the subscript f and s denote fluid and solid particles, respectively. It is obvious that both modified and unmodified models cannot simulate the peak pressure value and incidence accurately. The unmodified model overestimates the peak pressure while the modified model underestimates that. The predictive error of the peak pressure is about 35% for the unmodified model and about 11% for the modified model. Both models has incidence lag about 0.002 sec.

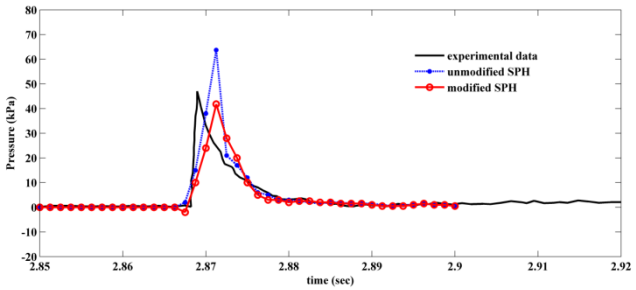

Figure 10. Time history of the estimated pressure at pressure gage P1 from modified and unmodified models compared with the experimental data from Yang et al. (2007)

4.3. Rotating Barge

As the third case study, a rectangular barge with one degree of freedom (roll motion) is simulated in a numerical wave flume with water depth of 0.9 m. The barge is 0.9 m in length, 0.3 m in width (B), 0.1 m in height, and with a draught (D) of 0.05 m (Fig. 11). A piston-type wave maker is used for generating a regular wave with a height of 0.06 m and a period (T) of 1.2 s. Besides, a sponge layer developed by Delavari and Gharabaghi (2014) is applied on the far end of the numerical flume to eliminate the effects of reflected waves. It is a modified version of a sponge layer which was previously developed by Yoon and Choi (2001) in a finite difference scheme which can be written as:

$$v(x) = exp\left[-\left(b^{-x/\Delta x} - b^{-x_s/\Delta x}\right)\ln(a.i_s)\right] \qquad (19)$$

where x is the position inside the sponge layer ($x = 0$ at the end of the flume), x_s is the width of the sponge layer, Δx is the particles spacing, a is a damping factor (here, $a = 2$), and i_s is introduced as the number of particles at the same elevation along a length equal to the wave length. Inside the sponge layer, velocities of the fluid particles are multiplied by Eq. (19). In the original equation, the parameter b is given by:

$$b = 1 + r_s + \exp\left(\frac{1}{r_s}\right) \qquad (20)$$

in which:

$$r_s = \frac{10}{i_s} \qquad (21)$$

In the numerical model, the particle spacing is 0.01 m and the fourth order Runge-Kutta scheme is used as a numerical integrator. The results of numerical model are compared with the experimental data from Jung (2004). Time history of the numerical (modified equation) and experimental water surface elevation (η), without the barge, is presented in Fig. 12. It can be seen that the numerical results are in good agreement with the experimental data (Jung, 2004). Also, Fig. 13 shows a snapshot of the velocity fields obtained from the numerical model simulated by the modified SPH scheme at $t = 35.2, 35.3,$ and $35.4\ s$. The results can be compare with the mean velocity profile in phases 2, 3, and 4 of the experimental ones. The experimental profiles are provided with the phase averaging from several instantaneous velocity measurements. We can see that the patterns of the fluid flow in the numerical results are almost identical with the experimental ones.

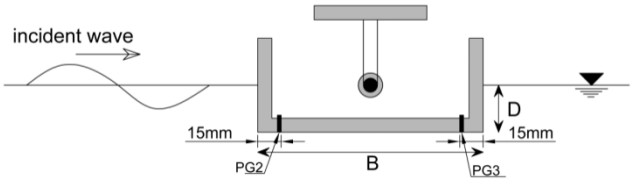

Figure 11. Schematic sketch of the rectangular barge

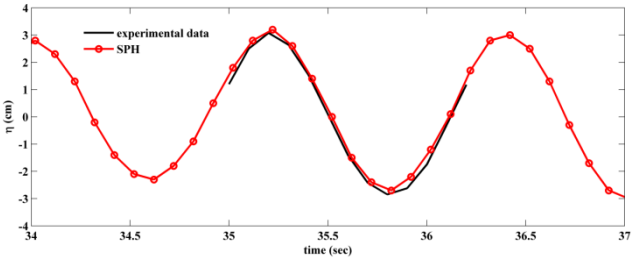

Figure 12. Time history of the estimated water surface elevation compared with the experimental data without the barge (experimental data from Jung, 2004)

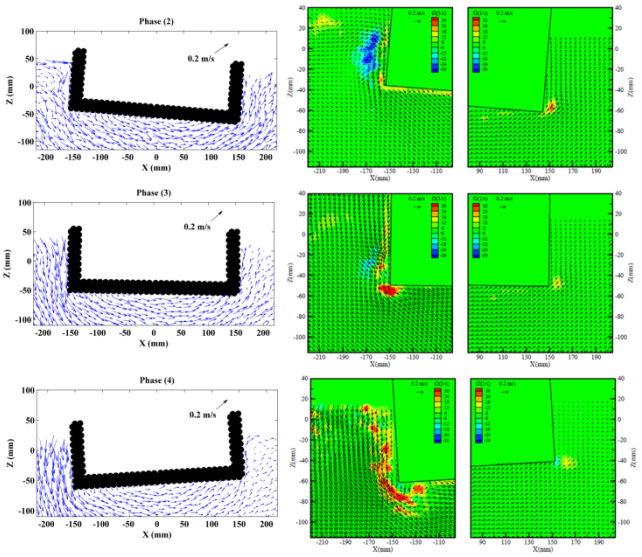

Figure 13. A snapshot of the velocity fields obtained from the numerical model simulated by the modified SPH scheme at $t = 35.2, 35.3,$ and $35.4\ s$ (left panels) and the mean velocity profiles in phases 2, 3, and 4 of the experimental data from Jung (2004) (right panels).

Numerical water surface elevations at the front and behind of the barge with roll motion with/without modification are shown in Figs. 14, and 15, respectively. The numerical results have been recorded at two points with a distance of 4 cm from the front and 6 cm from the behind of the barge in the wave flume. These results are compared with the experimental data (Jung, 2004).

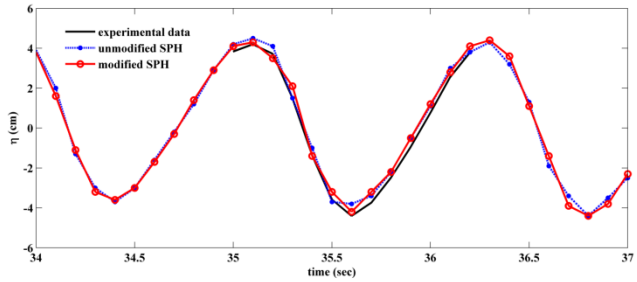

Figure 14. Time history of the estimated water surface elevation at the front of the barge with roll motion related to the modified and unmodified models compared with the experimental data (Jung, 2004)

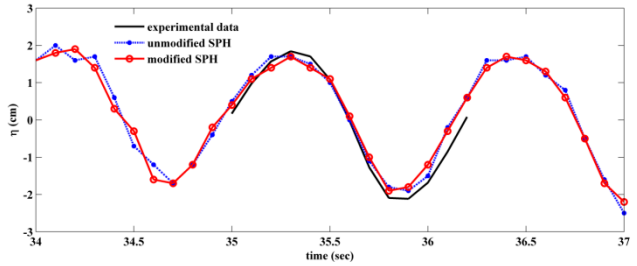

Figure 15. Time history of the estimated water surface elevation behind of the barge with roll motion related to the modified and unmodified model compared with the experimental data (Jung, 2004)

It can be seen that both models can simulate the superposition of incident waves with the reflected waves in front of the structure with good accuracy (Fig. 14). However, the results obtained from the modified model are almost in better agreements with the experimental data particularly near the crest and trough. However, the results related to the transmitted waves behind of the barge, in spite to their acceptable accuracy, needs to further improvement (Fig. 15).

Another parameter that was investigated is the wave-induced motions of the barge. The barge has one degree of freedom and can only rotate around its center of gravity. Results of the roll motion of the barge obtained from the modified and unmodified models have been presented in Fig. 16. It is obvious that the results obtained from the modified model are more accurate than those obtained from the unmodified one. The maximum error of the modified model is about 9% while it is about 19% for the unmodified model.

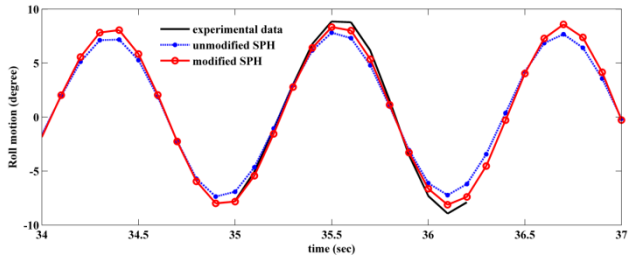

Figure 16. Time history of the roll motion of the barge obtained from the modified and unmodified models compared with the experimental results reported by Jung (2004)

Finally, the time history of the total pressure at gauges PG2 and PG3 (Fig. 11) has been shown in Figs. 17 and 18. From the figures, it can be seen that the results obtained from both of the models have some oscillations and considerable errors at the peak points. At gauge PG2, it is about 48% for the modified model and about 58% for the unmodified one. At gauge PG3, the results obtained from the modified model are more accurate, as its predicted error for the peak pressure is about 35% while it is about 62% for the unmodified model. The main part of these errors can be due to the origin of the WCSPH scheme that uses a state equation for calculating the pressure field.

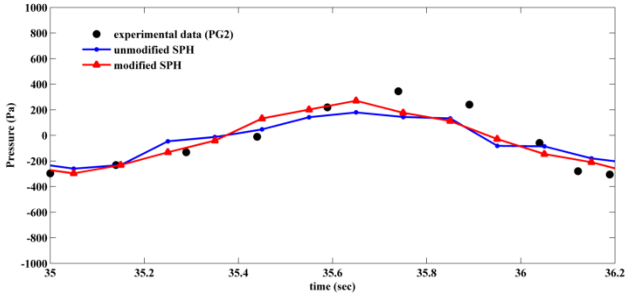

Figure 17. Time history of the total pressure at gauge PG2 obtained from the modified and unmodified models compared with the experimental results reported by Jung (2004)

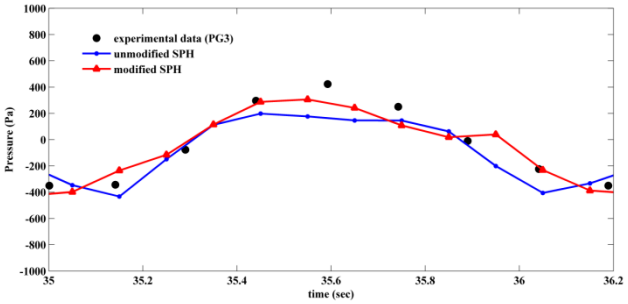

Figure 18. Time history of the total pressure at gauge PG3 obtained from the modified and unmodified models compared with the experimental results reported by Jung (2004)

4.4. Pile-supported floating Breakwater

As the last case, a rectangular floating breakwater supported by vertical piles is simulated in a numerical wave flume with water depth (d) of 0.3 m (Fig. 19). The breakwater has one degree of freedom (heave motion) and it can only moves in vertical direction. A piston-type wave maker is used for simulating a regular wave and similar to the previous case, a sponge layer (Delavari and Gharabaghi, 2014) is applied on the far end of the flume. According to the experimental work performed by Tolba (1998), numerical simulations have been performed with two different wave characteristics and two different dimensions of the structure. The heave motion of a breakwater with the dimensions of 0.3 m in length, 0.15 m in width (B), and draft (D) of 0.1 m due to the incident wave height (H) of 0.0462 m with a period (T) of 0.8 s is calculated. In the numerical model, the particle spacing is 0.006 m and the fourth order Runge-Kutta scheme is used as a numerical integrator. Figs. 20 presents a snapshot of the velocity field of the numerical model simulated by the modified SPH at $t = 6.5\ s$. Time history of the heave motion of the

studied breakwater has been compared with the experimental results of Tolba (1998) in Fig. 21. It can be seen that the predicted results by the modified model are considerably better than the results of the unmodified model.

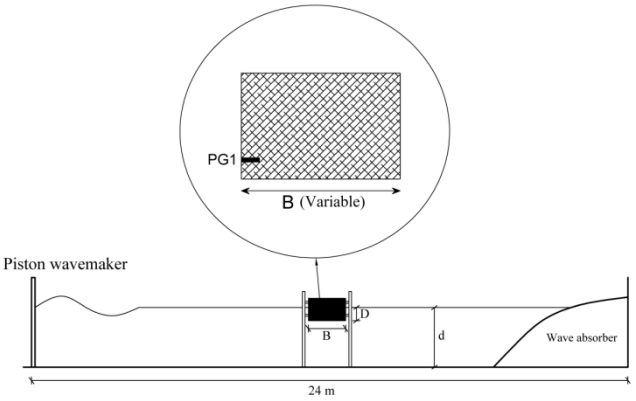

Figure 19. Schematic sketch of the rectangular pile-supported floating breakwater

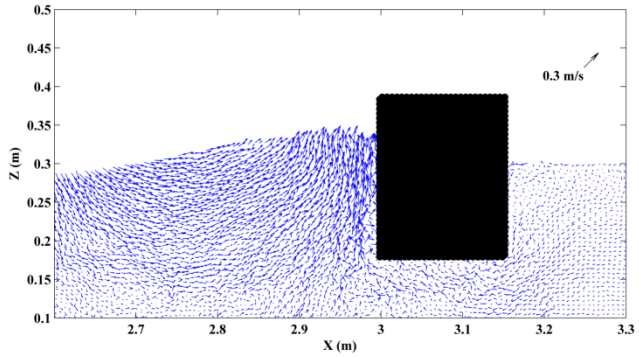

Figure 20. A snapshot of the velocity field of the numerical model simulated by the modified SPH scheme at $t = 6.5\ s$

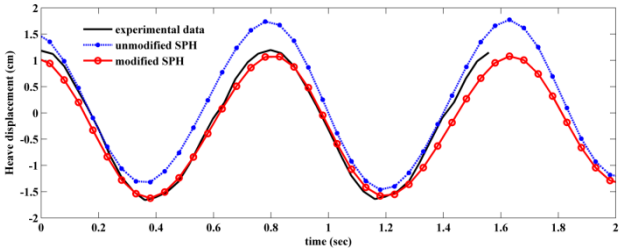

Figure 21. Time history of the heave motion of the pile-supported floating breakwater obtained from the modified and unmodified models compared with the experimental results reported by Tolba (1998)

In the next step, the pressure calculation for a pile-supported floating breakwater with dimensions of 0.3 *m* in length, 0.3 *m* in width, and a draft of 0.084 *m* is studied numerically under regular waves with height of 0.055 *m* and period (*T*) of 1.0. Fig. 22 shows the time history of the pressure at gauge PG1 (Fig. 19) calculated with both modified and unmodified models compared with the experimental data from Tolba (1998). The maximum predictive error of the modified SPH is about 72% while it is about 171% for the unmodified one. It can be seen that in spite of the results obtained from both models needs more improvement but the results of the modified model are in better agreement with the experimental data and there is no sudden increase in the pressure values.

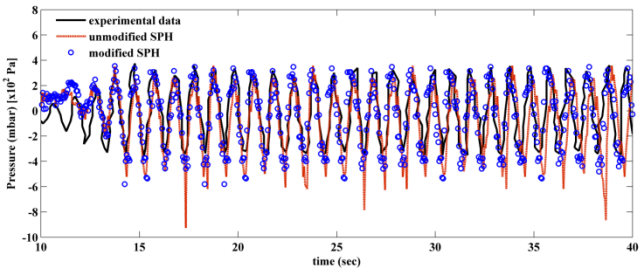

Figure 22. Time history of the calculated pressure obtained from the modified and unmodified models at gauge PG1 compared with the experimental results reported by Tolba (1998)

5. Conclusions

Simulation of the wave-structure interaction is one of the complicated and motivating fields in ocean engineering. In literature, there are several numerical solvers for Navier-Stokes' equations. Smoothed Particle Hydrodynamic (SPH) scheme as a simple solver scheme for this purpose has recently developed. In this paper, the repulsive force boundary method proposed by Monaghan and Kajtar (2009) has been modified in order to consider the effects of both fluid/solid particles' acceleration. The modified model is verified by simulating the violent interactions between waves and structures, therefore four test cases are simulated using WCSPH scheme and the results are compared with the experimental data. First, in order to evaluate the numerical viscous model, the lid-driven cavity problem was simulated. Also, a wedge water entry problem was investigated to evaluate the abilities of the modified fluid-solid interaction equation in simulating the wedge impact condition. Then, as a main purpose, the performance of the modified interaction force equation in calculating the violent interactions between waves and structures was investigated. In the next two test cases, the hydrodynamic parameters such as water surface elevation, motion response of the structure, and pressure distribution on the structure were estimated by the developed WCSPH scheme. First case was a rectangular barge with roll degree of freedom and second one was a pile-supported floating breakwater having only vertical motions. Results show that the modified model is more reliable than the unmodified one in simulating the violent wave-structure interaction problems.

6. References

1- Adami, S., Hu, X. Y. and Adams, N. A., (2012), *A generalized wall boundary condition for smoothed particle hydrodynamics*, Journal of Computational Physics, Vol. 231, p. 7057–7075.

2- Bouscasse, B., Colagrossi, A., Marrone, S. and Antuono, M., (2013), *Nonlinear water wave interaction with floating bodies in SPH*, Journal of Fluids and Structures, Vol. 42, p. 112-129.

3- Cao, X. Y., Ming, F. R. and Zhang, A, M., (2014), *Sloshing in a rectangular tank based on SPH simulation*, Applied Ocean Research, Vol. 47, p. 241-254.

4- Delavari, E. and Gharabaghi, A. R. M., (2014), *A modified sponge layer boundary condition for a numerical wave flume based on the SPH scheme*, The 11th Int. Conf. on Coasts, Ports and Marine Structures (ICOPMAS 2014), Tehran.

5- Faltinsen, O. M., (1977), *Numerical solution of transient nonlinear free-surface motion outside or inside moving bodies*, In: Proceedings Second Int. Conf. on Num. Ship Hydrodynamics, UC Berkeley, p. 257–266.

6- Gao, R., Ren, B., Wang, G. and Wang, Y., (2012), *Numerical modeling of regular wave slamming on surface of open-piled structures with the corrected SPH method*, Applied Ocean Research, Vol. 34, p. 173-186.

7- Ghia, U., Ghia, K. N. and Shin, C. T., (1982), *High-Re solutions for incompressible flow using the Navier-Stokes equations and a multigrid method*, Journal of Computational Physics, Vol. 48(3), p. 387-411.

8- Gomez-Gesteria, M., Rogers, B.D., Crespo, A.J.C., Dalrymple, R.A., Narayanaswamy, M. and Dominguez, J.M., (2012), *SPHysics-Development of a free surface fluid solver-part 1: Theory and formulations*, Computers and Geosciences, Vol. 48, p. 289-299.

9- Greenhow, M. and Lin, W-M., (1983), *Nonlinear free surface effects: Experiments and theory*, Report No. 83-19, Massachusetts Institute of Technology.

10- Hashemi, M. R., Fatehi, R. and Manzari, M. T., (2012), *A modified SPH method for simulating motion of rigid bodies in Newtonian fluid flows*, International Journal of Non-linear Mechanics, Vol. 47, p. 626-638.

11- Jung, K-H., (2004), *Experimental study on rectangular barge in beam sea*, Ph.D. Thesis, Texas A&M University.

12- Kajtar, J. B., (2009), *Smooth lattice general relatively and SPH simulations swimming linked bodies*, Ph.D. Thesis, Monash University.

13- Kajtar, J. and Monaghan, J. J., (2008), *SPH simulations of swimming linked bodies*, Journal of Computational Physics, 227, p. 8568-8587.

14- Kajtar, J. B. and Monaghan, J. J., (2010), *On the dynamics of swimming linked bodies*, European Journal of Mechanics B/Fluids, Vol. 29, p. 377-386.

15- Koo, W., (2003), *Fully nonlinear wave-body interactions by a 2D potential numerical wave tank*, Ph.D. Thesis, Texas A&M University.

16- Liu, M. B., Shao, J. R. and Li, H. Q., (2014), *An SPH model for free surface flows with moving rigid objects*, International Journal for Numerical Methods in Fluids, Vol. 74, p. 684-697.

17- Lo, E. Y. M. and Shao, S., (2002), *Simulation of nearshore solitary wave mechanics by an incompressible SPH method*, Applied Ocean Research, Vol. 24, p. 275-286.

18- Loverty, S. M., (2004), *Experimental hydrodynamics of spherical projectiles impacting on a free surface using high speed imaging techniques*, M.Sc. Thesis, Massachusetts Institute of Technology.

19- Monaghan, J. J., (1994), *Simulating free surface flows with SPH*, Journal of Computational Physics, Vol. 110, p. 399-406.

20- Monaghan, J. J., (2000), *SPH without a tensile instability*, Journal of Computational Physics, Vol. 159, p. 290-311.

21- Monaghan, J. J. and Kajtar, J. B., (2009), *SPH particle boundary forces for arbitrary boundaries*, Computer Physics Communications, Vol. 180, p. 1811-1820.

22- Monaghan, J. J. and Lattanzio, J. C., (1985), *A refined particle method for astrophysical problems*, Astronomy and Astrophysics, Vol. 149, p. 135-143.

23- Morris, J. P. and Fox, P. J., Y. Zhu, (1997), *Modeling low Reynolds number incompressible flows using SPH*, Journal of Computational Physics, Vol. 136, p. 214–226.

24- Ni, X., Feng, W. B. and Wu, D., (2014), *Numerical simulations of wave interactions with vertical wave barriers using the SPH method*, International Journal for Numerical Methods in Fluids, DOI:10.1002/fld.3933.

25- Omidvar, P., Stansby, P. K. and Rogers, B. D., (2012), *Wave body interaction in 2D using smoothed particle hydrodynamics (SPH) with variable particle mass*, International Journal for Numerical Methods in Fluids, Vol. 68, p. 686-705.

26- Omidvar, P., Stansby, P. K. and Rogers, B. D., (2013), *SPH for 3D Floating Bodies Using Variable Mass Particle Distribution*, International Journal for Numerical Methods in Fluids, Vol. 72 (4), p. 427-452.

27- Ren, B., He, M., Dong, P. and Wen, H., (2015), *Nonlinear simulations of wave-induced motions of a freely floating body using WCSPH method*, Applied Ocean Research, Vol. 50, p. 1-12.

28- Sun, H. and Faltinsen, O. M., (2006), *Water impact of horizontal circular cylinders and cylindrical shells*, Applied Ocean Research, Vol. 28, p. 299-311.

29- Sun, P., Ming, F. and Zhang, A., (2015), *Numerical simulation of interactions between free surface and rigid body using a robust SPH method*, Ocean Engineering, Vol. 98, p. 32-49.

30- Tolba, E. R. A. S., (1998), *Behaviour of floating breakwaters under wave action*, Ph.D. Thesis, Suez Canal University, Panama.

31- Valizadeh, A. and Monaghan, J. J., (2015), *A study of solid wall models for weakly compressible SPH*, Journal of Computational Physics, Vol. 300, p. 5-19.

32- Yan, R., Monaghan, J. J., Valizadeh, A. and Xu, F., (2015), *The effect of air on solid body impact with*

water in two dimensions, Journal of Fluids and Structures, Vol. 59, p. 146-164.

33- Yang, S. H., Lee, H. H., Park, T. H., Lee, I. H. and Lee, Y. W., (2007), *Experimental and numerical study on the water entry of symmetric wedges and a stern section of modern containership*, In: Proceedings of the 10th International Symposium on Practical Design of Ships and other Floating Structures (PRADS 2007), Houston, Texas, USA, p. 518-526.

34- Yettou, E-M., Desrochers, A. and Champoux, Y., (2006), *Experimental study on the water impact of a symmetrical wedge*, Fluid Dynamics Research, Vol. 38, p. 47-66.

35- Yoon, S. B. and Choi, J. W., (2001), *A Note on extension of fully dispersive weakly nonlinear wave equations for rapidly varying topography*, Coastal Engineering Journal, Vol. 43(3), p. 143-160.